
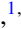














Examining the correlation between multi-neutron transfer and inelastic excitations in sub-barrier fusion enhancement

Anjali Rani ^{1,*}, S. Mandal ^{1,†}, K. Chakraborty ¹, R. Gupta ¹, C. V. Ahmad ¹, A. Parihari ¹, D. Vishwakarma ¹, P. Khandelwal¹, P. S. Rawat ¹, P. Sherpa ¹, S. Kumar ¹, N. Madhavan², S. Nath ², J. Gehlot², Rohan Biswas ², Gonika², Chandra Kumar ², Shoaib Noor ³ and A. Vinayak⁴

¹Department of Physics & Astrophysics, University of Delhi, New Delhi 110007, India

²Inter-University Accelerator Centre, Aruna Asaf Ali Marg, New Delhi 110067, India

³Thapar Institute of Engineering & Technology, Patiala, Punjab 147004, India

⁴Department of Physics, Karnatak University, Dharwad, Karnataka 580003, India



(Received 18 June 2022; accepted 16 November 2022; published 19 December 2022)

Background: Heavy-ion fusion cross-sections at sub barrier energies are found to be enhanced by orders of magnitude as compared to the predictions of one-dimensional barrier penetration model (1-D BPM). The coupling of various internal degrees of freedom has been employed to decrypt the mechanism responsible for the observed sub-barrier fusion enhancement. However, the unambiguous role of multi-neutron transfer channels in the sub-barrier domain is still elusive.

Purpose: We aim to explore and disentangle the effects of multi-neutron transfer channels from the inelastic excitations in the vicinity of the Coulomb barrier.

Method: The fusion excitation functions for $^{28}\text{Si} + ^{116,120,124}\text{Sn}$ systems were measured from $\approx 14\%$ below to $\approx 15\%$ above the Coulomb barrier by detecting the evaporation residues (ERs) at the focal plane of the Recoil Mass Separator (RMS), Heavy Ion Reaction Analyzer (HIRA) at the Inter-University Accelerator Centre (IUAC), New Delhi.

Results: The extracted fusion cross sections for the investigated systems at sub-barrier energies are significantly enhanced as compared to the predictions of 1-D BPM calculations. To probe the underlying mechanism responsible for the observed sub-barrier fusion enhancement, the coupled-channels (CC) formalism was employed. Coupled reaction channels (CRC) calculations by incorporating the one-neutron transfer channel to elucidate the significance of the transfer channel on the fusion dynamics were performed. Further, the semiempirical coupled channels (ECC) approach was explored to decipher the possible cause of the observed fusion excitation function trend. A systematic analysis of the neighboring systems available in the literature was also performed.

Conclusions: CC calculations were able to reproduce the measured fusion excitation functions for $^{28}\text{Si} + ^{116,120}\text{Sn}$ systems to a reasonable extent. However, observed sub-barrier fusion enhancement in $^{28}\text{Si} + ^{124}\text{Sn}$ system could not be explained using CC calculations. The influence of multi-neutron transfer channels was highlighted in the coupled-channels calculations. The interplay of collective excitations and neutron transfer was observed.

DOI: [10.1103/PhysRevC.106.064606](https://doi.org/10.1103/PhysRevC.106.064606)

I. INTRODUCTION

Despite extensive research in the past few decades, heavy-ion fusion reaction dynamics around the Coulomb barrier continue to be an active area of investigation [1–7]. In the simplest classical approach, fusion can take place only at energies above the barrier, which results from attractive nuclear and repulsive Coulomb potentials. However, fusion at sub-barrier energies is purely governed by the quantum mechanical penetration through the barrier. A substantial enhancement in the sub-barrier fusion cross sections over the predictions of one-dimensional barrier penetration model (1-D BPM) cal-

culations has been observed experimentally. The couplings between various internal degrees of freedom such as static and dynamic deformation of the colliding partners, viz., inelastic excitations, nucleon transfer channels, and neck formation, have been explored to understand the underlying reaction mechanism. The influence of inelastic excitations on sub-barrier fusion enhancement is quite well established within the framework of coupled-channels calculations [8–10]; however, the unambiguous role of transfer channels is still not fully understood [11–18]. The role of positive Q -value transfer channels in explaining the sub-barrier fusion data in Ni systems was first investigated by Broglia *et al.* [19]. This observation was then reaffirmed by quasielastic neutron transfer measurements for $^{58}\text{Ni} + ^{58,64}\text{Ni}$ systems [20]. The first quantitative description of the role of multi-neutron transfer channels on the fusion dynamics was performed with

*akadyan@physics.du.ac.in

†smandal@physics.du.ac.in

$^{58}\text{Ni} + ^{124}\text{Sn}$ systems [21,22]. To investigate the influence of channel couplings around the barrier, $^{40,48}\text{Ca}$, ^{32}S on $^{90,94,96}\text{Zr}$ systems have been extensively studied [6,23,24]. A vivid correlation between the low-lying collective states of the colliding nuclei and transfer channels in the sub-barrier fusion enhancement has been observed in these systems.

The coupling of transfer channels in the sub-barrier region has been examined through a comparison of radioactive Sn on Ni and stable Te on Ni systems, which have different ground state positive Q -value neutron transfer (PQNT) channels [25]. The reduced excitation functions have been found to be similar for the investigated Sn + Ni and Te + Ni systems, suggesting a strikingly different influence of positive Q -value transfer channels on the fusion process. A similar trend has also been observed for $^{60,64}\text{Ni}$ on ^{100}Mo [26], ^{64}Ni on ^{118}Sn [27], and $^{16,18}\text{O}$ on ^{118}Sn systems [28]. To address the effect of PQNT channels on sub-barrier fusion enhancement an exhaustive study was performed by our group with ^{28}Si on several isotopes of Zr, viz. $^{90,92,94,96}\text{Zr}$ [29,30], and ^{40}Ca on ^{70}Zn [31] systems. The fusion cross sections are relatively enhanced with the number of neutrons getting transferred outside the closed shell of Zr isotopes. Further, it has been stated that a clear role of the transfer channels can be observed in the systems with less deformed or nearly spherical interacting nuclei. Deb *et al.* [32] investigated the role of transfer channels in the vicinity of the Coulomb barrier with the $^{18}\text{O} + ^{116}\text{Sn}$ system, but an unambiguous role of PQNT channels could not be inferred from the measured fusion excitation functions. The measured fusion cross sections for systems $^{46,50}\text{Ti} + ^{124}\text{Sn}$ have been compared with those of $^{40}\text{Ca} + ^{124}\text{Sn}$ and $^{58}\text{Ni} + ^{124}\text{Sn}$ [33]. This comparison indicated the significance of positive Q -value transfer channels coupling on fusion in ^{40}Ca , $^{46}\text{Ti} + ^{124}\text{Sn}$ systems. Tripathi *et al.* [34,35] investigated the isotopic dependence and channel coupling effects in fusion of $^{16}\text{O} + ^{112,116}\text{Sn}$ and $^{32}\text{S} + ^{112,116,120}\text{Sn}$ systems. The significant contribution of coupling of collective excitations with multiphonon channels for the heavier systems was emphasized. The clear role of coupling to neutron transfer channels could not be deduced from the measurements. Fusion excitation functions for the reactions $^{124,132}\text{Sn}$ with $^{40,48}\text{Ca}$ using inverse kinematics have been measured [36]. $^{124,132}\text{Sn}$ on $^{40,48}\text{Ca}$ systems showed weak sub-barrier fusion enhancement which was explained by coupling to the low-lying 2^+ and 3^- states of the target and projectile. However, fusion cross sections for $^{124,132}\text{Sn} + ^{40}\text{Ca}$ were very strongly enhanced below the barrier. Although it appeared from the fusion measurements that the enhancement is solely due to the presence of large PQNT channels, the relative enhancement was not found to be proportional to the magnitudes of positive Q -values, which are much greater for $^{132}\text{Sn} + ^{40}\text{Ca}$ than for the $^{124}\text{Sn} + ^{40}\text{Ca}$ system. Recently, the fusion excitation function for $^{28}\text{Si} + ^{100}\text{Mo}$ was reinvestigated [37]. The influence of inelastic excitation, as well as of nucleon transfer channels, in sub-barrier fusion dynamics, was addressed. However, the explicit role of transfer channels in the fusion process could not be concluded from the measurements.

Even after numerous research efforts in the past few decades, the unambiguous role of PQNT channels in the sub-barrier fusion enhancement is still not established. In

the present article, we report the fusion measurements on $^{28}\text{Si} + ^{116,120,124}\text{Sn}$ systems. The fusion cross-sections have been extracted through the detection of ERs at the focal plane of the Heavy Ion Reaction Analyzer (HIRA) [38]. Sn isotopes are nearly spherical with a similar shell structure. The lowest quadrupole and octupole states are collective in nature and there are no marked differences in either the energy levels or deformation values for different Sn isotopes. Also, the aforementioned systems have varying ground state Q values for neutron transfer channels. Therefore, with the motivation to disentangle the effect of multi-neutron transfer channels from the inelastic excitations in the sub-barrier fusion enhancement, we have investigated ^{28}Si on Sn systems. Further, because Sn is a reservoir of neutrons, the effect of pairing correlation in connection with superfluidity effects can also be explored. Sn isotopes have extra neutrons outside their closed subshell resulting in the flow of neutrons between the colliding partners, which might take place either sequentially or simultaneously in the form of a cluster, which can further shed some light on the pairing correlation among the interacting nuclei. A brief account of the experimental methodology is presented in Sec. II. The results obtained along with the theoretical interpretations using coupled channels (CC), coupled reaction channels (CRC), and the semiclassical ECC approach are described in Sec. III. The systematic analysis of the various systems available in the literature is also presented in the same section. The work is summarized in Sec. IV.

II. EXPERIMENTAL DETAILS

The experiment was performed using a ^{28}Si pulsed beam with a pulse separation of 2 μs from the Pelletron accelerator at the Inter-University Accelerator Centre, New Delhi. Isotopically enriched $^{116,120,124}\text{Sn}$ targets of thickness ≈ 230 $\mu\text{g}/\text{cm}^2$ [39], ≈ 215 $\mu\text{g}/\text{cm}^2$, and ≈ 100 $\mu\text{g}/\text{cm}^2$, respectively fabricated on thin carbon backing of ≈ 20 $\mu\text{g}/\text{cm}^2$ using the vacuum evaporation technique, were used in the experiment. The isotopic enrichment of all Sn targets was more than 99%. Fusion excitation functions were measured in the laboratory beam energy range of 88–121 MeV spanning $\approx 14\%$ below to $\approx 15\%$ above the Coulomb barrier (V_B), with 1.5 MeV energy steps around the barrier and 2 MeV steps in the sub-barrier region. Two silicon detectors with a 1 mm diameter aperture were mounted inside the target chamber at 15.5° with respect to beam direction for beam monitoring and cross-section normalization. A carbon foil of thickness ≈ 10 $\mu\text{g}/\text{cm}^2$ was placed 10 cm downstream from the target for reequilibration of charge states of ERs. The ERs were dispersed at the focal plane of HIRA in accordance with their mass (A) to charge (q) ratio A/q . Fusion cross sections were extracted from the yield of ERs, which were separated from the scattered beam particles using HIRA. For the present experiment, HIRA was kept at zero degrees with respect to the beam direction and at a solid angle of acceptance 5 mSr. A position-sensitive multiwire proportional counter (MWPC) with an active area of 150×50 mm^2 , operated at a pressure of 5 mbar of isobutane gas, was placed at the focal plane of HIRA to detect the evaporation residues. The time of flight (ToF) was measured with the help of a time to amplitude converter (TAC) with

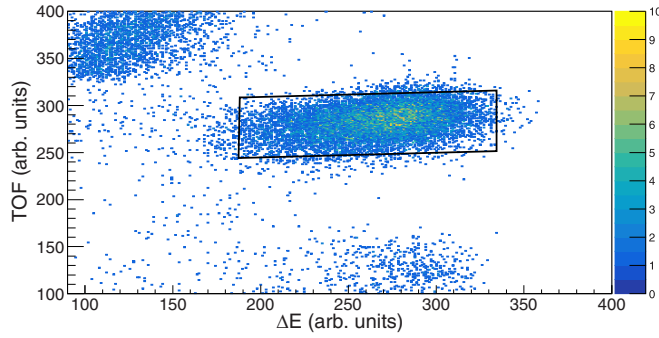


FIG. 1. Two-dimensional spectrum depicting the energy loss of reaction products in the MWPC vs time of flight for the $^{28}\text{Si} + ^{124}\text{Sn}$ system at $E_{\text{lab}} = 106$ MeV. The events within the rectangular gate represents ERs reaching the focal plane detector of the HIRA, which are clearly separated from the scattered beamlike particles.

an anode signal of the MWPC as the start and delayed radio frequency (RF) as the stop signal. This ToF resulted in the clear identification of ERs from multiple scattered beamlike particles through a two-dimensional spectrum of ToF vs ΔE (energy loss of ERs in MWPC). As a representative case, the ΔE -ToF spectrum for the $^{28}\text{Si} + ^{124}\text{Sn}$ system at $E_{\text{lab}} = 106$ MeV is shown in Fig. 1. The events within the rectangular gate represent ERs which are unambiguously separated from the scattered beamlike particles. HIRA was optimized through scanning for the most probable charge state, mass, and energy of ERs reaching the MWPC at $E_{\text{lab}} = 106$ MeV. The best set of values was obtained with the help of maximum transmission efficiency and clean separation of ERs from beamlike scattered particles. The experimentally measured ER cross section was considered as the fusion cross section since the fission contribution for the investigated systems is negligible in the present range of energies. The fusion cross section (σ_{fus} in mb) was estimated using the following expression:

$$\sigma_{\text{fus}}(E) = \left(\frac{Y_{\text{ER}}}{Y_M} \right) \left(\frac{d\sigma}{d\Omega} \right)_{\text{Ruth}} \Omega_M \frac{1}{\eta} \quad (1)$$

where Y_{ER} is the yield of ERs at the focal plane of HIRA detected by the MWPC, Y_M is the geometric mean of monitor yields, $\left(\frac{d\sigma}{d\Omega} \right)_{\text{Ruth}}$ is the differential Rutherford scattering cross section (mb/Sr) in the laboratory frame of reference, Ω_M is the solid angle subtended by the monitor detectors, and η is the average ER transmission efficiency of HIRA.

The accurate estimation of the transmission efficiency (η) of HIRA is an essential parameter for extraction of absolute σ_{ER} . It is defined as the ratio of the number of ERs reaching the focal plane to the total number of ERs emerging from the target. The efficiency (η) for the systems investigated in the present study was calculated using the semimicroscopic Monte Carlo code TERS [40,41] (within an uncertainty of 10%). The TERS code generates a distribution for energy, charge states, and angle of the residues based on the Monte Carlo method. The charge state distribution of the ERs was estimated in the code based on the empirical formula proposed by Nikolaev *et al.* [42,43]. These were further used to obtain the trajectory of ERs through the Recoil Mass Separator.

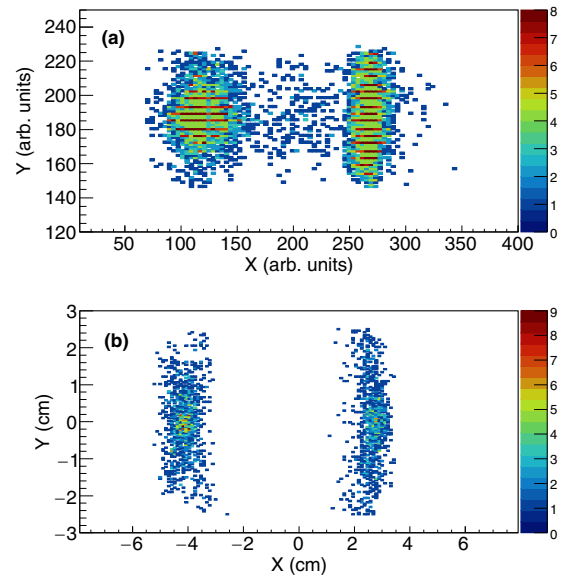


FIG. 2. The position spectrum obtained at the focal plane MWPC detector for (a) experiment and (b) simulation using TERS code for the $^{28}\text{Si} + ^{124}\text{Sn}$ system at $E_{\text{lab}} = 106$ MeV.

Further details regarding the simulation code can be found in Refs. [40,41]. Two charge states ($q = 14^+, 15^+$) of ERs were observed at the focal plane of HIRA and simulated using the code TERS. A comparison of the experimental spectrum [Fig. 2(a)] with the simulated spectrum obtained using TERS [Fig. 2(b)] for the mass/charge (A/q) distribution at the focal plane of HIRA for the $^{28}\text{Si} + ^{124}\text{Sn}$ system at $E_{\text{lab}} = 106$ MeV is shown in Fig. 2. The simulation was performed with 10^5 events of the projectile-target interaction. Two distinct groups correspond to two different charge states of evaporation residues. A clear agreement between the experimental and simulated spectra is observed in Fig. 2.

To estimate the average transmission efficiency of HIRA, a weighted average of the HIRA efficiencies was taken for relevant evaporation channels at all incident energies. The relative yield of different ERs channels was estimated from the statistical model code PACE4 [44]. The simulated range of η for the systems investigated in the energy range of 88–121 MeV is $\approx(4-7)\%$. The value of incident beam energies was corrected for the energy loss in carbon backing and half target thickness. The uncertainties associated with measured fusion cross section consist of statistical and systematical uncertainties, where η has the largest contribution in the latter.

III. DATA ANALYSIS AND RESULTS

A. CCFULL

The quantum mechanical coupled-channels formalism was employed in deciphering the mechanisms that are responsible for the experimentally observed enhancement in fusion cross sections at sub-barrier energies as compared to the predictions of 1-D BPM calculations [45]. The Akyüz-Winther (AW) parametrization of the Woods-Saxon potential was used for coupled-channels analysis in the present article [46]. The

TABLE I. Attractive nuclear potential parameters (V_0 , r_0 , a_0) along with the barrier parameters (V_B , R_B) for $^{28}\text{Si} + ^{116,120,124}\text{Sn}$ systems used in CC calculations.

System	V_B (MeV)	R_B (fm)	V_0 (MeV)	r_0 (fm)	a_0 (fm)
$^{28}\text{Si} + ^{116}\text{Sn}$	86.19	10.97	249.49	1.07	0.67
$^{28}\text{Si} + ^{120}\text{Sn}$	85.89	11.04	250.00	1.07	0.67
$^{28}\text{Si} + ^{124}\text{Sn}$	85.19	11.11	250.46	1.07	0.67

potential parameters for $^{28}\text{Si} + ^{120}\text{Sn}$ system were taken from Baby *et al.* [35]. The depth of the nuclear potential was adjusted to match the barrier position with the experimental fusion barrier. The set of potential parameters potential depth (V_0), radius (r_0), and diffuseness (a_0) along with the uncoupled barrier height and barrier radius used in CC calculations using the CCFULL program are tabulated in the Table I.

The experimentally measured fusion cross sections (σ_{fus}) plotted as a function of energy in the center-of-mass frame ($E_{\text{c.m.}}$) divided by the uncoupled barrier for $^{28}\text{Si} + ^{116,120,124}\text{Sn}$ systems are shown in Fig. 3. The fusion cross sections in the absence of any coupling were considered as the 1-D BPM cross-sections [shown by the continuous red line in Fig. 3(a)], which underpredict the experimentally obtained fusion cross-sections at the sub-barrier energies. Further, to investigate the channel coupling effects in the vicinity of the Coulomb barrier, collective states of colliding nuclei were incorporated into CC calculations. The low-lying inelastic states of the projectile and the target along with the corresponding deformation strength and excitation energies are listed in Table II [34,47–50]. The value of β_4 for ^{28}Si was taken from Ref. [51]. Sn nuclei are nearly spherical and exhibit a vibrational spectrum [52,53]. Hence, vibrational states of Sn isotopes were incorporated in the CC calculations. It is observed from Fig. 3(a) that the inclusion of the 2^+ vibrational state of the Sn target (green dotted line) in the CC calculation enhances the fusion cross sections as compared to 1-D BPM calculations but still underpredicts the experimental fusion cross sections. Further, the 3^- state of ^{116}Sn (pink dashed line) was also included in CC calculations.

It can be inferred from the fusion excitation plots that the 3^- state of Sn targets enhances the fusion cross-section more in magnitude than the 2^+ state of the targets, implying a

TABLE II. Excited states with their corresponding energies (E_J), spin, parity (J^π), and deformation parameters (β_J) used in the coupled-channels calculations.

Nucleus	J^π	E_J (MeV)	β_J
^{28}Si	2^+	1.779	-0.407
	4^+	4.617	0.10
^{116}Sn	2^+	1.293	0.111
	3^-	2.266	0.213
^{120}Sn	2^+	1.171	0.107
	3^-	2.40	0.176
^{124}Sn	2^+	1.131	0.095
	3^-	2.602	0.153

stronger coupling to the 3^- state. The coupled-channels calculations even after the inclusion of vibrational coupling of the Sn targets (2^+ , 3^-), were inadequate to explain the excitation functions in the sub-barrier region. Therefore, rotational states of ^{28}Si (blue dot-dash) were also added successively in the CC calculations. The inclusion of 2^+ states of the projectile ^{28}Si further enhances the sub-barrier fusion cross section. The fusion excitation function for $^{28}\text{Si} + ^{116}\text{Sn}$ system was well reproduced by the CCFULL calculations after the inclusion of the inelastic couplings (rotational for ^{28}Si and vibrational for ^{116}Sn), as shown in Fig. 3(a). For the case of ^{120}Sn [Fig. 3(b)], vibrational along with the rotational states of the colliding nuclei were insufficient to explain the fusion excitation function in the sub-barrier region. Therefore, mutual excitations of both projectile and target along with two phonon couplings, $^{120}\text{Sn}(2^+)^2 \otimes 3^-$; $^{28}\text{Si } 2^+, 4^+$ (red dashed line), for vibrational states were incorporated in the CC calculations. This brings an additional enhancement to the cross section but still is unable to reproduce the fusion cross section in the entire sub-barrier domain. Further, in an attempt to explain the underlying mechanism of the reaction dynamics, transfer channels were also included in CC calculations. In the CCFULL formalism, the effect of the pair transfer channel is incorporated through a simplistic transfer strength form factor F_{tr} . The inclusion of the transfer strength form factor with $F_{tr} = 0.3$ (green dash-dot line) gave a reasonable fit to the fusion excitation function in the entire energy range except deep below the barrier for ^{120}Sn , as shown in Fig. 3(b). The

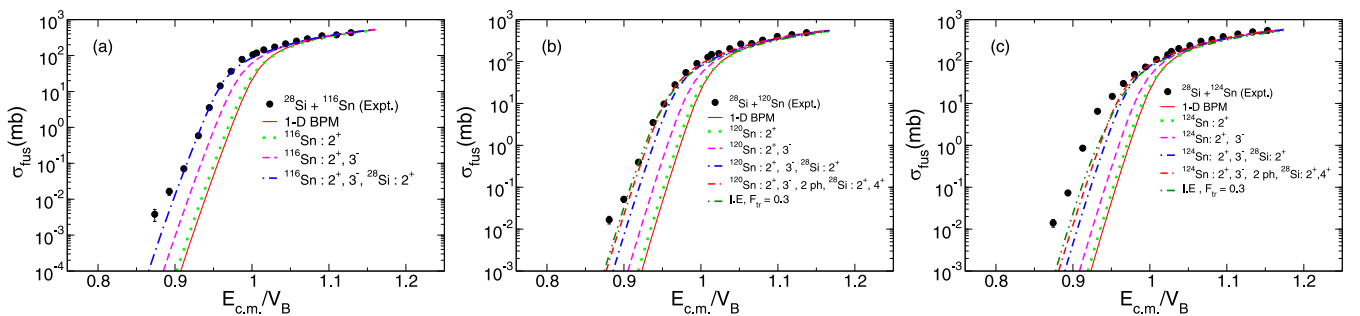


FIG. 3. Experimentally measured fusion excitation function for the (a) $^{28}\text{Si} + ^{116}\text{Sn}$, (b) $^{28}\text{Si} + ^{120}\text{Sn}$, and (c) $^{28}\text{Si} + ^{124}\text{Sn}$ systems along with uncoupled (1-D BPM) and coupled-channels calculations using the CCFULL program. The error bars on the higher energy side are within the size of the symbol.

TABLE III. The ground state Q -values (MeV) for various neutrons pickup (+) and stripping (−) channels for $^{28}\text{Si} + ^{116,120,124}\text{Sn}$ systems used in theoretical calculation.

System	+1n	+2n	+3n	+4n	+5n	+6n	−1n	−2n
$^{28}\text{Si} + ^{116}\text{Sn}$	−1.089	+1.973	−1.741	−0.286	−6.563	−7.220	−10.236	−14.22
$^{28}\text{Si} + ^{120}\text{Sn}$	−0.631	+3.494	+0.755	+3.012	−2.043	−2.074	−11.009	−15.50
$^{28}\text{Si} + ^{124}\text{Sn}$	−0.015	+4.64	+2.419	+5.449	+0.852	+1.882	−11.446	−16.571

strength of the transfer form factor (F_{tr}) was varied from 0.3 to 0.5, but a negligible effect was observed in the fusion cross section at sub-barrier energies. The variation of F_{tr} beyond 0.5 substantially underpredicted the fusion cross section at above-barrier energies. A coupling scheme similar to that adopted for the $^{28}\text{Si} + ^{120}\text{Sn}$ system fails to reproduce the fusion excitation function for the $^{28}\text{Si} + ^{124}\text{Sn}$ system even after the inclusion of one pair of neutron transfer channels along with inelastic couplings [Fig. 3(c)]. A marginal difference in the fusion cross section at sub-barrier energies was observed with $F_{tr} = 0.3$. The value of F_{tr} was varied further in an attempt to explain the experimentally obtained fusion excitation function for the $^{28}\text{Si} + ^{124}\text{Sn}$ system. It enhances the fusion cross section below the Coulomb barrier by an insignificant amount but underpredicts the cross section at higher energies. Therefore, even after the coupling of the transfer channel through varying coupling strengths, CCFULL was unable to explain the entire experimentally measured fusion excitation function for the $^{28}\text{Si} + ^{124}\text{Sn}$ system. One possible cause of this discrepancy might be the role of multi-neutron transfer channels in the sub-barrier fusion enhancement.

The ground state Q -values of the three systems (Table III) shows that the $^{28}\text{Si} + ^{116}\text{Sn}$ system has all negative ground state Q -values for neutron transfer channels except $2n$ pickup, while $^{28}\text{Si} + ^{120}\text{Sn}$ has $2n$ to $4n$ pickup channels having positive Q -value transfer channels and the $^{28}\text{Si} + ^{124}\text{Sn}$ reaction has positive Q -values up to $6n$ pickup channels. As is apparent from the fusion excitation plots for the three systems, the inelastic coupling enhances the sub-barrier fusion by an almost similar amount for each target. This similarity stems from collective properties of the $^{116,120,124}\text{Sn}$ targets having similar deformation strengths. An additional sub-barrier fusion enhancement in the case of $^{28}\text{Si} + ^{124}\text{Sn}$ system could be attributed to the presence of multi-neutron positive Q -value neutron transfer channels, which could not be accounted for properly in CCFULL.

B. Coupled reaction channel (CRC) calculations

Even after the extensive efforts to explain the discrepancy between the experimentally measured and theoretically predicted fusion cross sections, the quantitative description of this deviation is still ambiguous. This is mainly due to the inclusion of transfer channel coupling through a very simplistic approach via pair transfer in the CCFULL program and without proper knowledge of transfer coupling strengths. Further, with ^{28}Si as a deformed (oblate) projectile, the relative contribution of the inelastic excitations and transfer channels in enhancing the sub-barrier fusion cross section becomes more intricate. FRESKO [54,55] can include transfer couplings

along with inelastic excitations of the interacting nuclei in a much more realistic manner. Further, unlike CCFULL, the one-neutron transfer channel can be incorporated into the coupled reaction channels (CRC) calculations [56]. Therefore, to examine the effect of the $1n$ transfer channel coupling and inelastic excitation on the sub-barrier fusion enhancement in an independent manner, CRC calculations using the FRESKO program were performed for $^{28}\text{Si} + ^{124}\text{Sn}$ system.

Akyüz-Winther (AW) parametrization of the Woods-Saxon potential was used to calculate the real part of the potential. The imaginary part of the potential was kept as $W_0 \approx 20.0$ MeV, $r_w = 1.0$ fm, and $a_w = 0.4$ fm. The depth of the binding potentials was varied to obtain the binding energies of the composite (neutron + core) system. Single-neutron pickup channel coupling ($Q = -0.015$ MeV) along with the low-lying inelastic excitations of target and projectile (the same as used in the CCFULL calculation) were incorporated into CRC calculations. For $1n$ pickup channels, the ejectile ^{29}Si is assumed to be present in the ground state and the residue ^{123}Sn is also taken to be in the ground state or two low-lying excited states. The value of the spectroscopic amplitude for the various states involved in the CRC calculations was taken from Ref. [57].

The experimentally obtained fusion cross section along with CRC calculations including inelastic excitations and transfer coupling are shown in Fig. 4. The fusion cross section is enhanced after the inclusion of inelastic coupling of both projectile and target (red dashed line) as observed earlier with the CCFULL calculation. Further, $1n$ transfer coupling (green dot-dash line) enhances the fusion cross section,

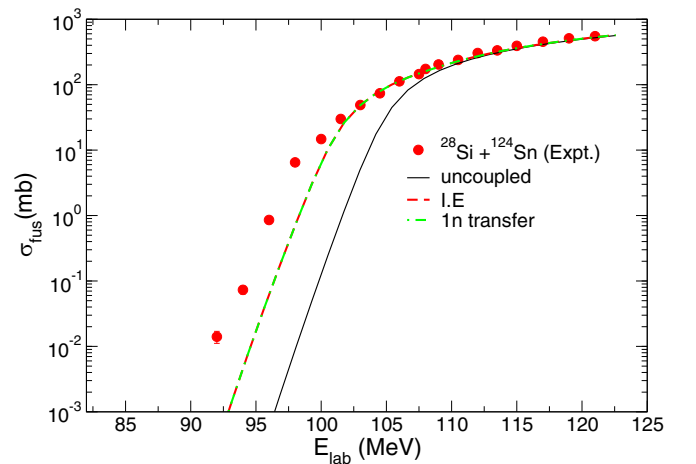


FIG. 4. Experimental fusion excitation function for the $^{28}\text{Si} + ^{124}\text{Sn}$ system along with coupled reaction channel (CRC) calculations using FRESKO program.

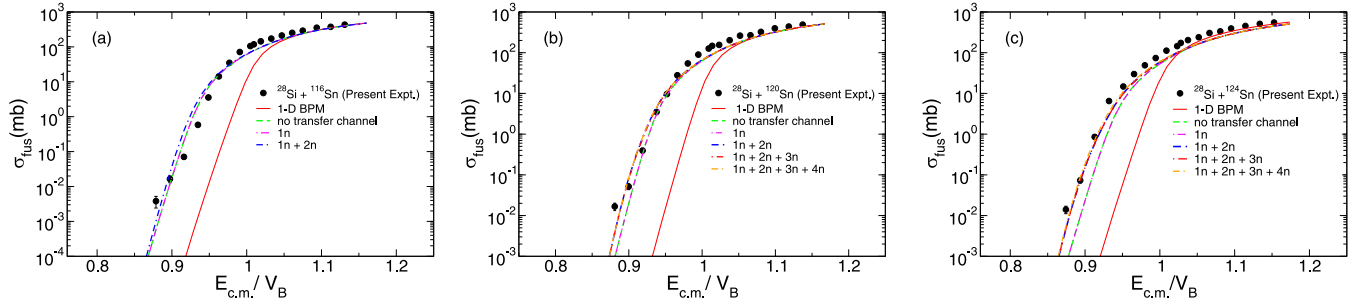


FIG. 5. Fusion excitation function for the (a) $^{28}\text{Si} + ^{116}\text{Sn}$, (b) $^{28}\text{Si} + ^{120}\text{Sn}$, and (c) $^{28}\text{Si} + ^{124}\text{Sn}$ systems along with the semi-classical calculations using the ECC program.

although not by a significant amount in magnitude at sub-barrier energies. The contribution of $1n$ transfer to the fusion cross section is almost similar to the collective effect of low-lying excited states of the participating nuclei. Therefore, it indicates that the role of neutron transfer channels in enhancing the fusion cross section at sub-barrier energies is crucial along with inelastic excitations. Since $^{28}\text{Si} + ^{124}\text{Sn}$ system has positive Q -values up to $6n$ pickup channels, we were constrained to perform complete CRC calculations with FRESKO for the present case. Therefore, an alternative semiclassical approach to extricate the effect of multi-neutron transfer channels at sub-barrier energies was adopted.

C. Semiclassical approach

An empirical coupled-channels (ECC) model based on the semiclassical approximation was proposed by Zagrebaev *et al.* [58,59]. It includes multi-neutron transfer channels along with the inelastic coupling for calculation of fusion cross sections. In this approach, the effect of neutron transfer channels was incorporated through the modified quantum penetration probability of the Coulomb barrier, which was calculated using the barrier distribution resulting from coupling of various channels. As tin isotopes have varying ground state positive Q -value neutron transfer channels, particularly for the $^{28}\text{Si} + ^{124}\text{Sn}$ system ($2n$ to $6n$), an attempt was made to investigate the effect of multi-neutron transfer channel coupling on the sub-barrier fusion enhancement using the semiclassical approach. The calculated fusion cross sections as a function of center of mass energies are plotted in Fig. 5.

The fusion cross sections in the absence of any coupling were calculated and shown by the red continuous line in Fig. 5. The green dashed line corresponds to the inelastic coupling of both projectile and target without inclusion of any neutron transfer channels. In the case of the $^{28}\text{Si} + ^{116}\text{Sn}$ system [Fig. 5(a)], only inelastic excitation without any transfer channel (green dashed line) gave a reasonable fit to the fusion excitation function, as observed earlier with the CCFULL calculation. The inclusion of neutron transfer channels slightly overestimates the fusion cross sections around the Coulomb barrier (blue dash-dot line) for the $^{28}\text{Si} + ^{116}\text{Sn}$ system. This system has all negative Q -value neutron transfer channels except $2n$ pickup. Hence, the nominal effect of the neutron transfer channel on the fusion cross sections around the Coulomb barrier might be expected. The $^{28}\text{Si} + ^{120,124}\text{Sn}$

systems have several neutron transfer channels with positive Q value. It was observed that the inclusion of multi-neutron transfer channels along with inelastic excitation is required to explain the experimentally measured fusion excitation functions for $^{28}\text{Si} + ^{120,124}\text{Sn}$ systems. In the case of the $^{28}\text{Si} + ^{124}\text{Sn}$ [Fig. 5(c)] system, the inelastic excitations alone are insufficient for explaining the sub-barrier fusion cross sections as observed with CCFULL as well as FRESKO calculations; therefore, neutron transfer channels were also incorporated successively into ECC calculations. The empirical approach (ECC) includes neutron transfer channels sequentially through the modified quantum penetration probability. The inclusion of the $1n$ transfer channel has a marginal effect on the fusion cross section (pink dot-dash line) depicted in our calculations with the FRESKO code also. The inclusion of the $2n$ transfer channel (blue dash-dot line) into empirical calculations gives substantial enhancement to the fusion cross section in the sub-barrier region but underpredicts the above-barrier cross section. Further addition of neutron transfer channels has minimal effect on the sub-barrier fusion cross sections. The effect of simultaneous $2n$ and $4n$ transfer channels seems to be more significant as compared to $1n$ and $3n$ transfer channels. The inclusion of $4n$ transfer channels (yellow dash-dot line) into ECC gave a reasonable fit to the fusion excitation function in the vicinity of the Coulomb barrier. The major contribution in the sub-barrier fusion enhancement was observed due to $2n$ transfer channels despite the presence of multi-neutron transfer channels with positive Q values. Similar results have also been reported in the literature [12,31,60].

D. Comparative analysis

To investigate the effect of PQNT channels on sub-barrier fusion enhancement, a comparative fusion excitation function for $^{28}\text{Si} + ^{116,120,124}\text{Sn}$ systems plotted on a reduced scale is shown in Fig. 6(a). Sn isotopes are nearly similar in their structural properties as depicted by their similar contributions through the inelastic excitations in the sub-barrier enhancement of all three isotopes. Therefore, the effect of multi-neutron transfer from the inelastic excitations in the sub-barrier fusion enhancement can be extricated through a reduced cross-section plot of three systems. The reduction of fusion cross section and energies was introduced to rule out the dependence of 1-D BPM cross section due to structural mismatch between various investigated systems [61].

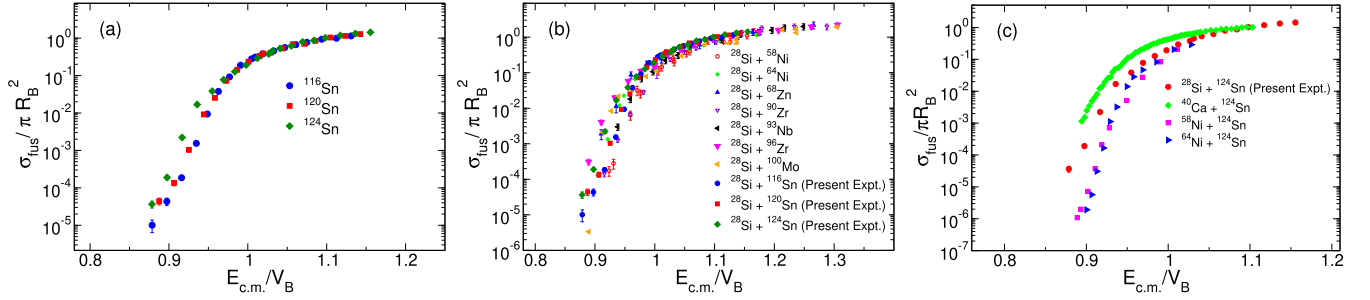


FIG. 6. Reduced fusion cross sections plotted as function of energy scaled as per the reduction procedure mentioned in the text for (a) $^{28}\text{Si} + ^{116,120,124}\text{Sn}$ systems, (b) for ^{28}Si as projectile with different targets available in literature [5,11,29,30], and (c) for ^{124}Sn target with different projectiles having varying deformation strength.

The fusion cross-sections were scaled with the corresponding geometrical cross section πR_B^2 (classical) and energies with the respective barrier height V_B .

It can be inferred from the reduced plot [Fig. 6(a)], that the fusion cross sections of $^{28}\text{Si} + ^{120,124}\text{Sn}$ systems are enhanced as compared to ^{116}Sn . The sub-barrier fusion cross section increases with the number of positive Q -value neutron transfer channels. This provides evidence of the role of multi-neutron transfer channels in the sub-barrier fusion enhancement. ^{124}Sn possesses four valence neutrons outside its closed subshell ($h_{11/2}$). These extra neutrons might result in the flow of neutrons between the colliding nuclei, viz., superfluidity effects in the case of ^{124}Sn , which might be responsible for an additional enhancement in the fusion cross section at sub-barrier energies. Further, to explore the structural effects along with the role of multi-neutron transfer channels in the sub-barrier region, a systematic study with various systems investigated in literature with ^{28}Si as projectile was performed. The reduced fusion cross sections as a function of reduced center-of-mass energies are shown in Fig. 6(b). It can be seen from the plot that the sub-barrier fusion enhancement is minimum for $^{28}\text{Si} + ^{58}\text{Ni}$ and ^{116}Sn (present study) systems which have negative Q -value neutron transfer channels. The maximum enhancement was observed in $^{28}\text{Si} + ^{96}\text{Zr}$ and ^{124}Sn (present study) systems, where multi-neutron positive Q -value neutron transfer channels are available, signaling toward the influence of multi-neutron transfer channels in the fusion dynamics. A similar comparative analysis with different projectiles having varying deformation strength studied for ^{124}Sn target was also performed. The reduction scheme is similar, as mentioned in the context of Fig. 6(a). It can be observed from Fig. 6(c) that ^{58}Ni and ^{64}Ni , which have similar ground state deformation strengths, show similar enhancement in the sub-barrier region. However, for ^{40}Ca , which is a spherical nucleus, the sub-barrier fusion enhancement is maximum as compared to ^{28}Si (present study), which is an oblate deformed projectile. This observation suggests that the effect of multi-neutron transfer channels can be observed more vividly with the spherical participating nuclei like ^{40}Ca , as observed in an earlier study [60].

IV. SUMMARY AND CONCLUSIONS

The fusion excitation function measurements for the $^{28}\text{Si} + ^{116,120,124}\text{Sn}$ systems around the Coulomb barrier were

carried out. A significant enhancement was observed in all three systems as compared to uncoupled (1-D BPM) calculations. Coupled-channels calculations were employed to explain the underlying mechanism of the reaction. The experimentally obtained fusion excitation functions for $^{28}\text{Si} + ^{116,120}\text{Sn}$ systems have been explained to a reasonable extent within the framework of CC calculations with inelastic excitations. Projectile excitations along with inelastic coupling of the target with two phonons seem to be a major contributing factor in fusion enhancement below the barrier in the case of $^{120,124}\text{Sn}$. However, sub-barrier fusion enhancement in $^{28}\text{Si} + ^{124}\text{Sn}$ system could not be explained even after taking into account one pair transfer coupling with varying transfer coupling strength in the CC calculations. These observations suggested the role of multi-neutron transfer channels coupling in the heavy ion fusion reactions. FRESKO calculations were performed to investigate the quantitative contribution of $1n$ transfer channel coupling along with the inelastic excitation of the interacting nuclei. The contribution of $1n$ transfer channel was observed with marginal effect in terms of magnitude. Further, to probe the underlying mechanism behind the observed enhancement in the fusion cross-sections below the barrier, a semiclassical approach was applied. The semiclassical treatment of analysis showed the relevance of multi-neutron transfer channels in the sub-barrier fusion enhancement. The inclusion of sequential $4n$ transfer channels in the ECC calculation gave a better fit to the $^{28}\text{Si} + ^{124}\text{Sn}$ excitation function. However, no set of coupling could reproduce the fusion excitation function in the entire energy domain. These findings indicate the need to incorporate multi-neutron transfer channel coupling along with the inelastic excitation simultaneously in the coupled-channels formalism. A systematic analysis with ^{28}Si as a projectile on various systems studied in literature along with ^{124}Sn with different projectiles was presented. The maximum sub-barrier fusion enhancement was observed with nearly spherical interacting nuclei. The neutron transfer cross-section measurements of the systems investigated in the present study might provide deeper insights into the influence of transfer channels on the fusion dynamics.

ACKNOWLEDGMENTS

The authors would like to acknowledge the IUAC Pelletron team for providing a stable ^{28}Si beam of required energies.

We are thankful to the target development laboratory of IUAC for the help and guidance during target fabrication. S.M. and A.R. would like to acknowledge the partial funding assistance

received from the Science and Engineering Research Board SERB (CRG/2018/003012) and IOE(FRP/PCMS/2020/27), University of Delhi.

- [1] A. B. Balantekin and N. Takigawa, *Rev. Mod. Phys.* **70**, 77 (1998).
- [2] B. B. Back, H. Esbensen, C. L. Jiang, and K. E. Rehm, *Rev. Mod. Phys.* **86**, 317 (2014).
- [3] M. Dasgupta, D. J. Hinde, N. Rowley, and A. M. Stefanini, *Annu. Rev. Nucl. Part. Sci.* **48**, 401 (1998).
- [4] R. G. Stokstad, Y. Eisen, S. Kaplanis, D. Pelte, U. Smilansky, and I. Tserruya, *Phys. Rev. Lett.* **41**, 465 (1978).
- [5] A. M. Stefanini, G. Fortuna, A. Tivelli, W. Meczynski, S. Beghini, C. Signorini, S. Lunardi, and M. Morando, *Phys. Rev. C* **30**, 2088 (1984).
- [6] A. M. Stefanini, L. Corradi, A. M. Vinodkumar, Y. Feng, F. Scarlassara, G. Montagnoli, S. Beghini, and M. Bisogno, *Phys. Rev. C* **62**, 014601 (2000).
- [7] P. Stelson, *Phys. Lett. B* **205**, 190 (1988).
- [8] R. N. Sahoo, M. Kaushik, A. Sood, P. Kumar, A. Sharma, S. Thakur, P. P. Singh, P. K. Raina, M. M. Shaikh, R. Biswas, A. Yadav, J. Gehlot, S. Nath, N. Madhavan, V. Srivastava, M. K. Sharma, B. P. Singh, R. Prasad, A. Rani, A. Banerjee *et al.*, *Phys. Rev. C* **99**, 024607 (2019).
- [9] J. R. Leigh, M. Dasgupta, D. J. Hinde, J. C. Mein, C. R. Morton, R. C. Lemmon, J. P. Lestone, J. O. Newton, H. Timmers, J. X. Wei, and N. Rowley, *Phys. Rev. C* **52**, 3151 (1995).
- [10] J. D. Bierman, P. Chan, J. F. Liang, M. P. Kelly, A. A. Sonzogni, and R. Vandenbosch, *Phys. Rev. Lett.* **76**, 1587 (1996).
- [11] D. O. Kataria, A. K. Sinha, J. J. Das, N. Madhavan, P. Sugathan, L. T. Baby, I. Mazumdar, R. Singh, C. V. K. Baba, Y. K. Agarwal, A. M. Vinodkumar, and K. M. Varier, *Phys. Rev. C* **56**, 1902 (1997).
- [12] V. V. Sargssyan, G. G. Adamian, N. V. Antonenko, W. Scheid, and H. Q. Zhang, *Phys. Rev. C* **91**, 014613 (2015).
- [13] J. O. Newton, C. R. Morton, M. Dasgupta, J. R. Leigh, J. C. Mein, D. J. Hinde, H. Timmers, and K. Hagino, *Phys. Rev. C* **64**, 064608 (2001).
- [14] V. I. Zagrebaev, *Phys. Rev. C* **67**, 061601(R) (2003).
- [15] V. Denisov, *Eur. Phys. J. A* **7**, 87 (2000).
- [16] H. Jia, C. Lin, L. Yang, X. Xu, N. Ma, L. Sun, F. Yang, Z. Wu, H. Zhang, Z. Liu *et al.*, *Phys. Lett. B* **755**, 43 (2016).
- [17] N. Prasad, A. Vinodkumar, A. Sinha, K. Varier, D. Sastry, N. Madhavan, P. Sugathan, D. Kataria, and J. Das, *Nucl. Phys. A* **603**, 176 (1996).
- [18] L. S. Danu, B. K. Nayak, E. T. Mirgule, R. K. Choudhury, and U. Garg, *Phys. Rev. C* **89**, 044607 (2014).
- [19] R. Broglia, C. Dasso, S. Landowne, and G. Pollarolo, *Phys. Lett. B* **133**, 34 (1983).
- [20] K. E. Rehm, F. L. H. Wolfs, A. M. van den Berg, and W. Henning, *Phys. Rev. Lett.* **55**, 280 (1985).
- [21] C. L. Jiang, K. E. Rehm, H. Esbensen, D. J. Blumenthal, B. Crowell, J. Gehring, B. Glagola, J. P. Schiffer, and A. H. Wuosmaa, *Phys. Rev. C* **57**, 2393 (1998).
- [22] H. Esbensen, C. L. Jiang, and K. E. Rehm, *Phys. Rev. C* **57**, 2401 (1998).
- [23] G. Montagnoli, S. Beghini, F. Scarlassara, A. M. Stefanini, L. Corradi, C. J. Lin, G. Pollarolo, and A. Winther, *Eur. Phys. J. A* **15**, 351 (2002).
- [24] A. M. Stefanini, F. Scarlassara, S. Beghini, G. Montagnoli, R. Silvestri, M. Trotta, B. R. Behera, L. Corradi, E. Fioretto, A. Gadea, Y. W. Wu, S. Szilner, H. Q. Zhang, Z. H. Liu, M. Ruan, F. Yang, and N. Rowley, *Phys. Rev. C* **73**, 034606 (2006).
- [25] Z. Kohley, J. F. Liang, D. Shapira, R. L. Varner, C. J. Gross, J. M. Allmond, A. L. Caraley, E. A. Coello, F. Favela, K. Lagergren, and P. E. Mueller, *Phys. Rev. Lett.* **107**, 202701 (2011).
- [26] A. M. Stefanini, G. Montagnoli, F. Scarlassara, C. L. Jiang, H. Esbensen, E. Fioretto, L. Corradi, B. B. Back, C. M. Deibel, B. Di Giovine, J. P. Greene, H. D. Henderson, S. T. Marley, M. Notani, N. Patel, K. E. Rehm, D. Sewerinyak, X. D. Tang, C. Ugalde, and S. Zhu, *Eur. Phys. J. A* **49**, 63 (2013).
- [27] C. J. Lin, H. M. Jia, H. Q. Zhang, X. X. Xu, F. Yang, L. Yang, P. F. Bao, L. J. Sun, and Z. H. Liu, *EPJ Web Conf.* **66**, 03055 (2014).
- [28] P. Jacobs, Z. Fraenkel, G. Mamane, and I. Tserruya, *Phys. Lett. B* **175**, 271 (1986).
- [29] S. Kalkal, S. Mandal, N. Madhavan, E. Prasad, S. Verma, A. Jhingan, R. Sandal, S. Nath, J. Gehlot, B. R. Behera, M. Saxena, S. Goyal, D. Siwal, R. Garg, U. D. Pramanik, S. Kumar, T. Varughese, K. S. Golda, S. Muralithar, A. K. Sinha *et al.*, *Phys. Rev. C* **81**, 044610 (2010).
- [30] Khushboo, S. Nath, N. Madhavan, J. Gehlot, A. Jhingan, N. Kumar, T. Banerjee, G. Kaur, K. Rojeeta Devi, A. Banerjee, Neelam, T. Varughese, D. Siwal, R. Garg, I. Mukul, M. Saxena, S. Verma, S. Kumar, B. R. Behera *et al.*, *Phys. Rev. C* **96**, 014614 (2017).
- [31] M. S. Khushboo, S. Mandal, N. Madhavan, S. Muralithar, J. J. Das, S. Nath, A. Jhingan, J. Gehlot, B. Behera, S. Verma, H. Singh, S. Kalkal, and R. Singh, *EPJ Web Conf.* **163**, 00029 (2017).
- [32] N. K. Deb, K. Kalita, H. A. Rashid, S. Nath, J. Gehlot, N. Madhavan, R. Biswas, R. N. Sahoo, P. K. Giri, A. Das, T. Rajbongshi, A. Parihari, N. K. Rai, S. Biswas, Khushboo, A. Mahato, B. J. Roy, A. Vinayak, and A. Rani, *Phys. Rev. C* **102**, 034603 (2020).
- [33] J. F. Liang, J. M. Allmond, C. J. Gross, P. E. Mueller, D. Shapira, R. L. Varner, M. Dasgupta, D. J. Hinde, C. Simenel, E. Williams, K. Vo-Phuoc, M. L. Brown, I. P. Carter, M. Evers, D. H. Luong, T. Ebadi, and A. Wakhle, *Phys. Rev. C* **94**, 024616 (2016).
- [34] V. Tripathi, L. T. Baby, J. J. Das, P. Sugathan, N. Madhavan, A. K. Sinha, P. V. Madhusudhana Rao, S. K. Hui, R. Singh, and K. Hagino, *Phys. Rev. C* **65**, 014614 (2001).
- [35] L. T. Baby, V. Tripathi, J. J. Das, P. Sugathan, N. Madhavan, A. K. Sinha, M. C. Radhakrishna, P. V. Madhusudhana Rao, S. K. Hui, and K. Hagino, *Phys. Rev. C* **62**, 014603 (2000).
- [36] J. J. Kolata, A. Roberts, A. M. Howard, D. Shapira, J. F. Liang, C. J. Gross, R. L. Varner, Z. Kohley, A. N. Villano, H. Amro, W. Loveland, and E. Chavez, *Phys. Rev. C* **85**, 054603 (2012).
- [37] A. M. Stefanini, G. Montagnoli, M. D'Andrea, M. Giacomini, C. Dehman, R. Somasundaram, V. Vijayan, L. Zago, G. Colucci, F.

- Galtarossa, A. Goasduff, and J. Grebosz, *J. Phys. G: Nucl. Part. Phys.* **48**, 055101 (2021).
- [38] A. Sinha, N. Madhavan, J. Das, P. Sugathan, D. Kataria, A. Patro, and G. Mehta, *Nucl. Instrum. Methods Phys. Res., Sect. A* **339**, 543 (1994).
- [39] N. K. Deb, K. Kalita, P. K. Giri, S. R. Abhilash, G. R. Umamathy, R. Biswas, A. Das, D. Kabiraj, S. Chopra, and M. Bhuyan, *J. Radioanal. Nucl. Chem.* **326**, 97 (2020).
- [40] S. Nath, *Comput. Phys. Commun.* **179**, 492 (2008).
- [41] S. Nath, *Comput. Phys. Commun.* **180**, 2392 (2009).
- [42] V. Nikolaev and I. Dmitriev, *Phys. Lett. A* **28**, 277 (1968).
- [43] R. Sagaidak and A. Yeremin, *Nucl. Instrum. Methods Phys. Res., Sect. B* **93**, 103 (1994).
- [44] A. Gavron, *Phys. Rev. C* **21**, 230 (1980).
- [45] K. Hagino, N. Rowley, and A. Kruppa, *Comput. Phys. Commun.* **123**, 143 (1999).
- [46] R. A. Broglia and A. Winther, *Heavy Ion Reactions*, (Benjamin Cummings, San Francisco, 1981).
- [47] S. Raman, C. W. Nestor, Jr., and P. Tikkanen, *At. Data Nucl. Data Tables* **78**, 1 (2001).
- [48] T. Kibedi and R. Spear, *At. Data Nucl. Data Tables* **80**, 35 (2002).
- [49] P. Möller, A. Sierk, T. Ichikawa, and H. Sagawa, *At. Data Nucl. Data Tables* **109-110**, 1 (2016).
- [50] S. Sinha, M. R. Pahlavani, R. Varma, R. K. Choudhury, B. K. Nayak, and A. Saxena, *Phys. Rev. C* **64**, 024607 (2001).
- [51] B. K. Nayak, R. K. Choudhury, A. Saxena, P. K. Sahu, R. G. Thomas, D. C. Biswas, B. V. John, E. T. Mirgule, Y. K. Gupta, M. Bhike, and H. G. Rajprakash, *Phys. Rev. C* **75**, 054615 (2007).
- [52] J. Bryssinck, L. Govor, V. Y. Ponomarev, F. Bauwens, O. Beck, D. Belic, P. von Brentano, D. De Frenne, T. Eckert, C. Fransen, K. Govaert, R. D. Herzberg, E. Jacobs, U. Kneissl, H. Maser, A. Nord, N. Pietralla, H. H. Pitz, and V. Werner, *Phys. Rev. C* **61**, 024309 (2000).
- [53] A. Bohr and B. Mottelson, *Nuclear Structure* (Benjamin, New York, 1975).
- [54] I. J. Thompson, *Comput. Phys. Rep.* **7**, 167 (1988).
- [55] <http://www.fresco.org.uk/>.
- [56] T. Tamura, *Rev. Mod. Phys.* **37**, 679 (1965).
- [57] D. G. Fleming, *Can. J. Phys.* **60**, 428 (1982).
- [58] V. I. Zagrebaev, V. V. Samarin, and W. Greiner, *Phys. Rev. C* **75**, 035809 (2007).
- [59] <http://nrv.jinr.ru/>.
- [60] V. A. Rachkov, A. V. Karpov, A. S. Denikin, and V. I. Zagrebaev, *Phys. Rev. C* **90**, 014614 (2014).
- [61] L. F. Canto, D. R. M. Junior, P. R. S. Gomes, and J. Lubian, *Phys. Rev. C* **92**, 014626 (2015).